Multiscale hydraulic modeling of the ITER TF he inlets during nominal and off-normal operation

Multi-Scale Hydraulic Modeling of the ITER TF He Inlets During Nominal and Off-Normal Operation

Laura Savoldi, Roberto Bonifetto, Arnaud Foussat, Marco Nenni, Vincenzo Santoro and Roberto Zanino, *Senior Member, IEEE*

***Abstract*—In ITER, the supercritical helium (SHe) coolant enters the superconducting toroidal field (TF) coils from the bore of the magnet, each inlet feeding two adjacent pancakes. Here, as a complement to and extension of experimental measurements performed by other authors, we address the issue numerically through a 3D CFD ("micro-scale") study of an ITER TF inlet, in both nominal and backflow conditions (like, e.g., in the case of a quench of the coil). The localized pressure drop at the inlet turns out to be relatively small. Nevertheless, for demonstration purposes of the multi-scale approach, suitable correlations for the localized pressure drop are derived, and then implemented in a lumped parameter component, to be used in the 4C system code for the "macro-scale" analysis of the entire TF coil and related cryogenic cooling loops.**

***Index Terms*— Nuclear fusion, ITER, Superconducting magnets, Supercritical helium, CFD.**

I. Introduction

THE safe planning of the operation of present and future fusion experiments using superconducting (SC) magnets should significantly benefit of the availability of system-level tools able, e.g., to reliably predict if for a given desired plasma scenario the needed temperature margin is maintained or not, if the magnet can be suitably protected in the case of a quench, etc. Such tools must be able to simultaneously and efficiently model the "macro" scale, i.e., the magnets, including winding and structures, if any, and the respective cryogenic circuits, including all the different details at the "micro" scale among which, of particular relevance here, the inlets of the supercritical helium (SHe) coolant.

In the ITER SC toroidal field (TF) coils and central solenoid (CS) [1], the SHe coolant enters from the bore of the magnet, at the transition between adjacent pancakes [2]. The SHe inlet in the CS and in a TF inlet mock-up, both with the basic features of a T-junction, have been recently analyzed in the case of normal operation using computational fluid dynamics (CFD) [3], as this approach had proven in the past to be rather successful for the derivation of thermal-hydraulic correlations (e.g., for the friction factor) in CICC [4], [5], The CFD model was proven in [6], by comparison with the available measurements [2], to be a reliable tool to assess the localized pressure drop Δp as well as the distribution of the mass flow rate in the different parts (petals, central channel) of the superconducting cable.

Here we develop a CFD model, based on the OpenFoam® software [7] and briefly described in Section II, for the full hydraulic characterization of an actual ITER TF inlet, which differs in several details from the previously studied mock-up [6]. Both the case of nominal operation, when the inlet actually feeds the pancakes with fresh SHe, and the case when, as in a fast discharge or a quench, the localized and possibly asymmetric He pressurization in a pancake gives rise to backflow in the T-junction, are considered.

First we consider nominal operation and the hydraulic characteristic of the inlet, in terms of localized pressure drop coefficient, is derived from steady-state numerical experiments.

Second, we investigate the case of backflow from the pancakes fed by the inlet. Two conditions are considered, namely when both pancakes sharing the inlet experience backflow, as during a fast discharge, and therefore flow reversal occurs also at the inlet, and when backflow occurs in only one of the two pancakes, as more likely during a quench, which may or may not result in flow reversal at the inlet. In all different situations a correlation for the localized pressure drop is obtained.

Following the approach proposed in [8], the correlations derived via "micro-scale" CFD analysis for the different situations considered above are then used to implement a lumped parameter component modeling the inlet in the "macro-scale" (system) code 4C [9], which was already used for the study of several types of transients in the ITER TF [10].

II. Micro-Scale (CFD) Inlet Model

The ITER TF inlet geometry is similar to that of the TF inlet mock-up considered in [6], see Fig. 1, except for small differences in the holes drilled in the grids and for the fact that, in the case of the actual TF inlet, the petal wrapping is removed below the inlet grids, to guarantee a more

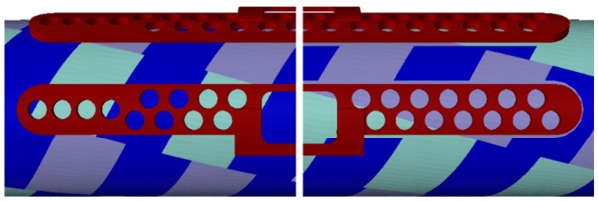

(a) (b)

Fig. 1. Detail of the grid directly below the inlet pipe: (a) inlet mock-up considered in [2]; (b) actual ITER TF inlet considered in this paper. The petal wrapping is shown in dark blue.

Manuscript received August 12, 2014.

L. Savoldi, R. Bonifetto, M. Nenni, V. Santoro and R. Zanino are with Dipartimento Energia, Politecnico di Torino, Torino, I-10129 Italy (phone: +39 011 090 4447; fax: +39 011 090 4499; e-mail: laura.savoldi@polito.it).

A. Foussat is with ITER IO, Cadarache, France.

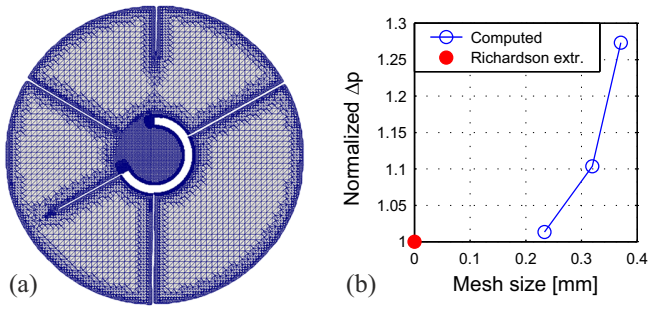

Fig. 2. (a) Cross section of the refined mesh used in the present analysis for the region away from the inlet (the central region contains a more refined mesh close around the central channel); (b) (Normalized) pressure drop across the inlet as a function of the *average* mesh size, estimated as $(V_{fluid}/\#\ cells)^{1/3}$, computed on three different meshes and compared with the Richardson extrapolation.

homogeneous flow distribution among the petals.

As in [6], the computational domain of the CFD model includes 0.6 m of conductor on each side of the TF inlet (the inlet grids are ~11.4 cm long), and a small portion of the inlet pipe (0.3 m long). Only the fluid domain is considered: the cable is modeled as an anisotropic porous medium, where the transverse permeability is reduced with respect to the longitudinal one by a factor of 100, as resulting from the analysis in [6].

Three different meshes (a coarse one of 14.5 MCells, an intermediate one of 23 MCells, and a refined one of 60 MCells, shown in Fig. 2a) have been developed for the analysis, and the grid independence has been checked considering a nominal inlet mass flow rate of 16 g/s of helium at 4.5 K and 0.5 MPa. The results in terms of computed inlet pressure drop on the three meshes have been compared with the Richardson extrapolation [11] based on the medium and fine meshes, as shown in Fig. 2b. The refined grid, showing a difference below 1% from the results computed by the Richardson extrapolation, has then been chosen to carry on the analysis presented below.

Different flow conditions have been addressed in this study:

A. normal operation (Fig. 3a), with possible flow unbalance within the two pancakes;
B. flow reversal in both pancakes (Fig. 3b), with possible flow unbalance;
C. flow reversal in one pancake only, with backflow in the inlet pipe (Fig. 3c);
D. flow reversal in one pancake only, with normal flow direction in the inlet pipe (Fig. 3d), for the sake of completeness.

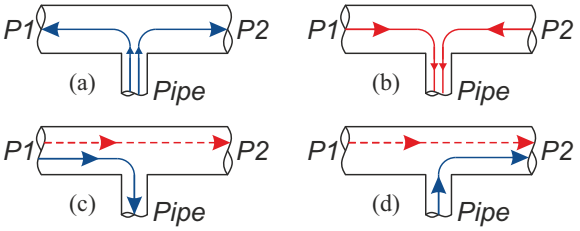

Fig. 3. Schematic view of the different situations considered for the CFD analysis of the TF inlet: (a) normal operation, case A; (b) reverse flow operation, case B; (c, d) hybrid operation, cases C and D, respectively. "P1", "P2" label the two pancakes on the same double pancake, fed by the common inlet "Pipe". The arrows indicate the direction of the flow.

In the different cases, different boundary conditions are imposed at the actual inlets/outlets, imposing the mass flow rate at the actual inlet(s) and the pressure at the actual outlet(s). The (total) inlet mass flow rate is varied in a range from ~6 g/s to at least ~22 g/s in all cases. If two outlets are present, the pressure of one of the two is kept fixed at 0 Pa (relative), while the other is varied in order to explore different flow unbalances.

The output of the simulations is post-processed in terms of computed pressure at the inlet(s) and average speed on the cross sections at the outlet(s).

III. Results and Discussion

In order to develop the characterization of the inlet from the computed results, we use the Bernoulli equation, which can be applied following the fluid streamlines from the actual inlet(s) to the actual outlet(s) [12], assuming negligible potential head and constant density.

A. *Localized pressure drop in Case A and B*

In Case A, the Bernoulli equation can be applied along the streamline in Fig. 3a, giving:

$$p_{Pipe} + \rho\frac{\bar{v}_{Pipe}^2}{2} = p_P + \rho\frac{\bar{v}_P^2}{2} + \rho {K_{Loc}}^A \frac{\bar{v}_P^2}{2} \quad (1)$$

$${K_{Loc}}^A = 2\frac{p_{Pipe}-p_P}{\rho\bar{v}_P^2} + \frac{\bar{v}_{Pipe}^2}{\bar{v}_P^2} - 1 \quad (2)$$

where the subscripts refer to the different sections shown in Fig. 3 (P is either P1 or P2 in case of symmetric flow), while the superscripts refer to the different cases (A or B).

Note that the localized pressure drop is written as a function of a dimensionless coefficient (K_{Loc}) and of the average speed of the fluid *in the pancake* where the streamline exits. This choice is driven by the final use of the computed characteristic in a system code, see Section IV below).

In Case B, the Bernoulli equation can be applied along the streamline in Fig. 3b, giving:

$$p_P + \rho\frac{\bar{v}_P^2}{2} - \rho {K_{Loc}}^B \frac{\bar{v}_P^2}{2} = p_{Pipe} + \rho\frac{\bar{v}_{Pipe}^2}{2} \quad (3)$$

$${K_{Loc}}^B = 2\frac{p_P-p_{Pipe}}{\rho\bar{v}_P^2} - \frac{\bar{v}_{Pipe}^2}{\bar{v}_P^2} + 1 \quad (4)$$

${K_{Loc}}^A$ and ${K_{Loc}}^B$ are computed post-processing the simulation results, and plotted in Fig. 4 as a function of the fraction of mass

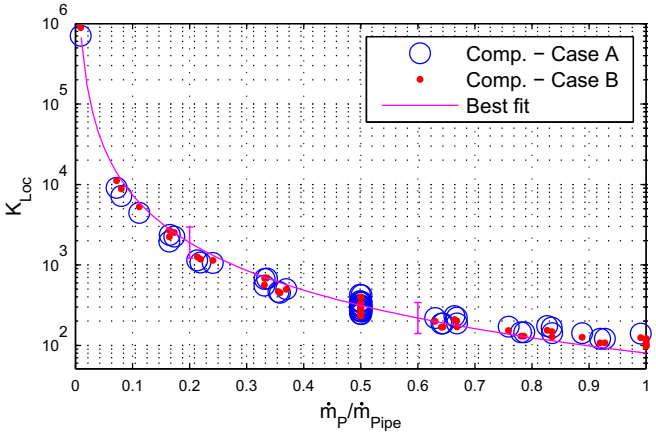

Fig. 4. K_{Loc} computed from the simulations of Case A (open circles) and Case B (dots), together with their best fit (with respective error bar).

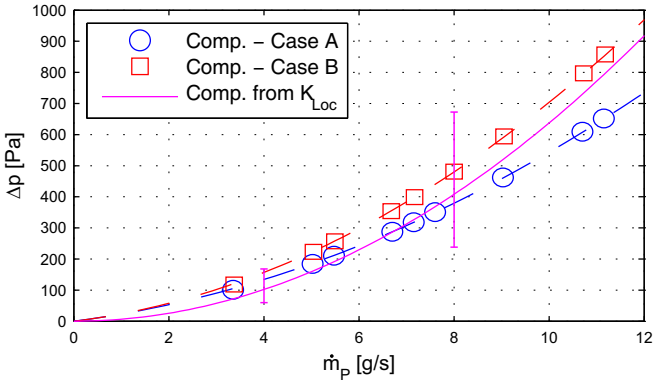

Fig. 5. Comparison between the operating point computed with the CFD simulations in Case A and B, and the results obtained using the best fit for the K_{Loc} evaluated for the same cases.

flow in one pancake over the total in the inlet pipe (this choice will allow to derive a single expression for K_{Loc}, valid for a wide range of mass flow rates). Mainly in view of the porous medium nature of the cable, a single correlation for K_{Loc} can be developed from the numerical database:

$$K_{Loc}{}^{A,B} = 80.122 \left(\frac{\dot{m}_P}{\dot{m}_{Pipe}}\right)^{-1.9663} \quad (5)$$

which fits the entire CFD dataset for both cases A and B with a $R^2 = 0.99$, and it is applicable for a mass flow rate in the inlet pipe up to ~22 g/s.

If we focus on the series of points with balanced mass flow rate (i.e., same mass flow rate to or from the two adjacent pancakes), $\left(\frac{\dot{m}_P}{\dot{m}_{Pipe}}\right) = 0.5$, we note a spread around the fit value, with K_{Loc} varying by a factor of 2 depending on the value of $\dot{m}_{Pipe}$. It is interesting for those points to assess the accuracy of Eq. (5), deriving from it the localized pressure drop Δp_{Loc} across the inlet at the different mass flow rates

$$\Delta p_{Loc} = \rho K_{Loc} \frac{\bar{v}_P^2}{2} \quad (6)$$

and comparing it to the Δp_{Loc} resulting directly from the CFD.

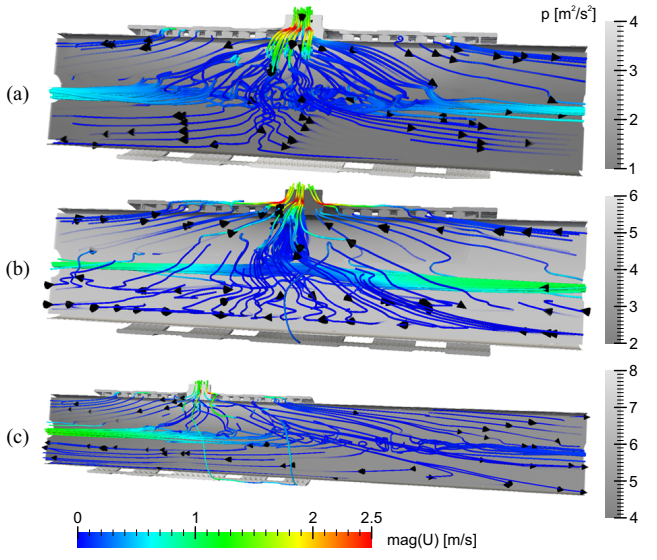

Fig. 6. Pathlines (colored according to the He speed) and pressure distribution in the inlet region: (a) pipe acting as inlet; (b) pipe acting as outlet with balanced mass flow; (c) pipe acting as inlet with unbalanced mass flow.

The comparison is presented in Fig. 5, that shows Eqs. (5,6) give a prediction of the pressure drop at the nominal mass flow rate (8 g/s) within 20% of that extracted directly from the CFD results. Although the localized pressure drop at the inlet is small in relative terms (equivalent to ~ 2 m of conductor), the derived correlation(s) will be used below to practically demonstrate an application of the multi-scale approach.

Looking at the computed flow and pressure fields in the inlet region (Fig. 6), it is possible to see that, when the flow is balanced (Figs. 6a-b), the flow path is, as expected, roughly symmetric in the two pancakes. However, when the pipe behaves as a common outlet (in the case of balanced reverse flow from both pancakes, Fig. 6b) the region where the He flows from the central channel to the outlet pipe is much more localized below the pipe itself (where the two opposite flows hit each other) than in the case in which the pipe is a real inlet (Fig. 6a). In the cases of unbalanced flow with the pipe acting as an inlet, the asymmetric behavior in the two channels is evident (stagnation point no more under the inlet grid), justifying the trend in Fig. 4 (different K_{Loc} computed at different mass flow unbalance), see Fig. 6c.

B. *Localized pressure drop in Case C and D*

In Case C, the Bernoulli equation can be applied along the solid streamline in Fig. 3c, using Eqs. (3) and (4), while in Case D, Eqs. (1) and (2) apply again for the solid streamline in Fig. 3d. The results are collected in Fig. 7, where the abscissa is $\dot{m}_{P1}/\dot{m}_{Pipe}$ for Case C and $\dot{m}_{P2}/\dot{m}_{Pipe}$ for Case D. The resulting best fit is

$$K_{Loc}{}^{C,D} = 93.109 \left(\frac{\dot{m}_P}{\dot{m}_{Pipe}}\right)^{-0.1625} \quad (7)$$

which fits the entire CFD dataset for cases C and D.

The pressure drop from one pancake to the adjacent one, in Cases C and D, can also be translated in terms of a localized pressure drop for Case C as

$$p_{P1} + \rho \frac{\bar{v}_{P1}^2}{2} = p_{P2} + \rho \frac{\bar{v}_{P2}^2}{2} + \rho K_{CC} \frac{\bar{v}_{P2}^2}{2} \quad (8)$$

$$K_{CC} = 2 \frac{p_{P1} - p_{P2}}{\rho \bar{v}_{P2}^2} + \frac{\bar{v}_{P1}^2}{\bar{v}_{P2}^2} - 1 \quad (9)$$

and for Case D as:

$$p_{P1} + \rho \frac{\bar{v}_{P1}^2}{2} - \rho K_{CC} \frac{\bar{v}_{P1}^2}{2} = p_{P2} + \rho \frac{\bar{v}_{P2}^2}{2} \quad (10)$$

$$K_{CC} = 2 \frac{p_{P1} - p_{P2}}{\rho \bar{v}_{P1}^2} - \frac{\bar{v}_{P2}^2}{\bar{v}_{P1}^2} + 1 \quad (11)$$

If we rearrange the results as a function of the ratio between

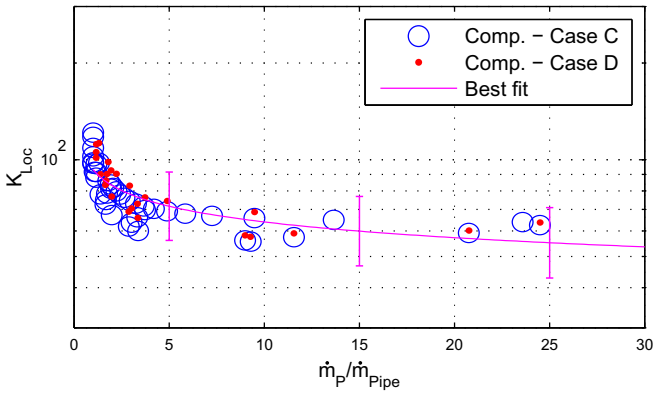

Fig. 7. K_{Loc} computed from the simulations of Case C (open circles) and Case D (dots), together with their best fit.

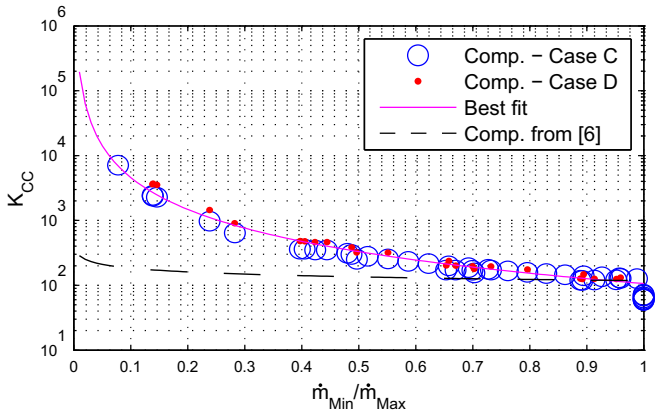

Fig. 8. K_{CC} computed from the simulations of Case C (open circles) and Case D (dots), together with their best fit. The equivalent value of K_{CC} computed from the distributed pressure drop in [6] is also reported.

minimum and maximum mass flow rate, we get the behavior plotted in Fig. 8, where a single excellent fit can be found as

$$K_{CC} = 106.47 \left(\frac{\dot{m}_{Min}}{\dot{m}_{Max}}\right)^{-1.6351} \quad (12)$$

In Fig. 8, K_{CC} is also computed for Case C starting from the distributed pressure loss in pseudo-dimensionless form (for the definitions of f^* (m^{-5}) and Re^* (m) see [6]), giving

$$K_{CC} = 2 \cdot 10^6 A_{P2}^2 f_{P2}^* L + \frac{\bar{v}_{P1}^2}{\bar{v}_{P2}^2} - 1 \quad (13)$$

where A is the He flow area in the conductor cross section.

Fig. 8 shows that, in the case of a plugged inlet pipe (i.e., same mass flow rate in P1 and P2), K_{CC} gives the pressure drop of the distributed friction factor along the conductor, as expected since at that point a constant mass flow rate is flowing in the conductor as the inlet could be ignored. For values of $\frac{\dot{m}_{Min}}{\dot{m}_{Max}} < 1$, Eq. (13) returns a lower value than Eq. (12), since in Eq. (13) f^* refers to the pancake with $\dot{m}_{Min}$ (and consequently the lowest Re* and the minimum K_{LOC}).

IV. Application of the Micro-Scale Results to Macro-Scale Analysis

As described in Section I and following the rationale explained in [6], the three correlations (5), (7) and (12), derived via CFD for K_{Loc} and K_{CC} in the different situations considered above, have been implemented in the lumped parameter characterization of the TF inlet used in the 4C code [9], which can be applied to the macro-scale analysis of an entire ITER TF coil [10], see Fig. 9. Each inlet pipe feeds a small inlet manifold

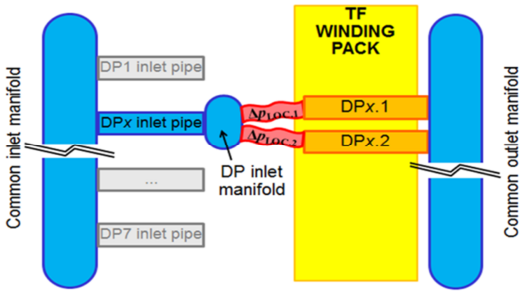

Fig. 9. 4C macro-scale model of a TF coil, including the He inlets with localized pressure drops evaluated using the correlations obtained from the micro-scale analysis of the He inlets.

for each double pancake (DP), corresponding to the portion of the inlet pipe included in the CFD model: the Δp obtained introducing in Eq. (6) the value of K_{Loc} from the correlations above and the average velocity at the inlet of each pancake (frozen at the previous time step) is added at each time step to the pressure drop computed for each pancake. With respect to [10], a centrifugal cold circulator was introduced in the TF winding cooling circuit, to connect the pressured drop along the pancakes with the mass flow rate. The computed localized inlet pressure drop induces as expected only a very small perturbation in the mass flow rate when steady state operation is considered as here.

V. Conclusion

A detailed CFD model of the ITER TF coil He inlets has been developed and applied to the characterization of the localized pressure drop. The pressure drop turns out to be small in relative terms (equivalent to ~ 2 m of conductor). Nevertheless, a set of correlations has been derived, valid for different situations (normal and reverse flow, balanced and unbalanced flow in the two pancakes fed by the same inlet), exploring a wide range of mass flow rate values, in order to fully demonstrate a practical application of the multi-scale approach [8].

The correlations derived via CFD have been implemented in a new circuit component to be used in the 4C macro-scale model.

Acknowledgment

We should like to gratefully acknowledge the computational resources provided by Helios - Computational Simulation Centre at the International Fusion Energy Research Centre, Rokkasho, Japan (http://www.iferc.org/csc/csc.html) and by HPC@POLITO, a project of Academic Computing within the Department of Control and Computer Engineering at the Politecnico di Torino, Italy (http://www.hpc. polito.it).

We thank the three anonymous reviewers for their careful reading of and suggestions on the first version of the manuscript.

References

[1] N. Mitchell, A. Devred, P. Libeyre, B. Lim, F. Savary, and ITER Magnet Division, “The ITER magnets: design and construction status”, *IEEE Trans. Appl. Supercond.*, vol. 22, no. 3, p. 4200809, Jun. 2012.

[2] C. Boyer, K. Seo, K. Hamada, A. Foussat, M. Le Rest, N. Mitchell, P. Decool, F. Savary, S. Sgobba, and K.-P. Weiss, “Validation of Helium Inlet Design for ITER Toroidal Field Coil,” *IEEE Trans. Appl. Supercond.*, vol. 24, no. 3, p. 3800504, Jun. 2014.

[3] R. Zanino, N. Martovetsky, A. Pasquali, L. Savoldi Richard, and D. Speziani, “Computational thermal-hydraulic analysis of the helium inlet options for the ITER Central Solenoid,” *IEEE Trans. Appl. Supercond.*, vol. 22, no. 3, p. 4902505, Jun. 2012.

[4] R. Zanino, S. Giors and R. Mondino, “CFD modeling of ITER Cable-in-Conduit Superconductors. Part II: Effects of spiral geometry on the central channel pressure drop”, Fus. Eng. Des., vol. 81, pp. 2605-2610, 2006.

[5] R. Zanino, S. Giors, L. Savoldi Richard, “CFD model of ITER CICC. Part VI: heat and mass transfer between cable region and central channel”, Cryogenics, vol. 50, pp. 158-166, 2010.

[6] R. Zanino, C. Boyer, A. Foussat, K. Hamada, M. Nenni, V. Santoro, K. Seo, and L. Savoldi Richard, “Computational Fluid Dynamics (CFD)

analysis of the Helium inlet mock-up for the ITER TF superconducting magnets," *IEEE Trans. Appl. Supercond*., vol. 24, no. 3, p. 4202405, Jun. 2014.
[7] http://www.openfoam.org/
[8] R. Zanino and L.Savoldi Richard, "Multiscale Approach and Role of Validation in the Thermal-Hydraulic Modeling of the ITER Superconducting Magnets," *IEEE Trans. Appl. Supercond.*, vol. 23, no. 3, p. 4900607, Jun. 2013.
[9] L. Savoldi Richard, F. Casella, B. Fiori, and R. Zanino, "The 4C code for the cryogenic circuit conductor and coil modeling in ITER," *Cryogenics*, vol. 50, pp. 167-176, 2010.
[10] L. Savoldi Richard, R. Bonifetto, A. Foussat, N. Mitchell, K. Seo, and R. Zanino, "Mitigation of the Temperature Margin Reduction due to the Nuclear Radiation on the ITER TF Coils," *IEEE Trans. Appl. Supercond*., vol. 23, no. 3, p.4201305, Jun. 2013.
[11] J. H. Ferziger, and M. Perić, *Computational Methods for Fluid Dynamics.* Springer, 2002.
[12] B. R. Munson, T. H. Okiishi, W. W. Huebsch, and A. P. Rothmayer, *Fluid Mechanics*. John Wiley and Sons, 2013.